



CrossMark
click for updates

Cite this: *RSC Adv.*, 2015, 5, 35425

Synthesis of polyethylene glycol-functionalized multi-walled carbon nanotubes with a microwave-assisted approach for improved heat dissipation†

Ahmad Amiri,^{*a} Rad Sadri,^a Goodarz Ahmadi,^b B. T. Chew,^a S. N. Kazi,^{*a} Mehdi Shanbedi^{*c} and Maryam Sadat Alehashem^d

In order to improve the dispersibility of multi-walled carbon nanotubes (MWCNT) in aqueous media, MWCNT were functionalized with tetrahydrofurfuryl polyethylene glycol (TFPEG) in a one-pot, fast and environmentally friendly method. To reduce defects and eliminate the acid-treatment stage, an electrophonic addition reaction under microwave irradiation was employed. Surface functionalization was analyzed by FTIR, Raman spectroscopy, thermogravimetric analysis (TGA). In addition, the morphology of TFPEG-treated MWCNT (PMWCNT) was investigated by transmission electron microscopy (TEM). After the functionalization phase, the convective heat transfer coefficient and pressure drop in PMWCNT-based water nanofluids with various weight concentrations were analyzed and compared with that of the base fluid. The results suggest that the addition of PMWCNT into the water improved the convective heat transfer coefficient significantly. The pressure drop of prepared PMWCNT-based water nanofluids showed an insignificant variation as compared with the base fluid and could result from good dispersivity of PMWCNT. According to the laminar flow results, as the weight concentration and Reynolds number increase, the convective heat transfer coefficient and pressure drop increase.

Received 12th February 2015
Accepted 13th April 2015

DOI: 10.1039/c5ra02736e

www.rsc.org/advances

1. Introduction

Energy optimization plays a vital role in different fields such as infrastructure, industry, defense *etc.* To fully realize energy optimization, different kinds of cooling systems with various designs have been employed over the past century.^{1–3} It is obvious that convective heat transfer can be considered as one of the most significant parameters in energy saving, especially in a majority of thermal equipment which commonly work with base fluids such as water, ethylene glycol, and different kinds of oils.^{2,4–7} In order to enhance conventional heat transfer of base fluids, the addition of highly thermally conductive nanoparticles such as metal, carbon, and metal oxides into the base fluids was introduced as an appropriate technique.^{8–13} Recently, a novel type of fluid, so-called nanofluid that includes

nanostructures has been introduced, and different types of nanofluids have been prepared by researchers. These fluids have shown attractive properties such as good stability, suitable thermal conductivity and high heat transfer coefficient. Since the time that the concept of nanofluids was introduced by Choi,^{14,15} numerous scientists studied the effects of presence of nanoparticles in various base liquids on their thermos-physical properties. In particular, considerable attention was given to the influence of nanoparticle concentration on the thermal conductivity and heat transfer coefficients of base fluids. Different carbon nanostructures like carbon nanotubes (CNT), graphene, fullerene and metal nanoparticles like copper (Cu) and aluminum oxide (Al₂O₃) have been used to enhance the thermal properties of nanofluids.^{9,10,16–20}

It is known that the thermal conductivity of most carbon particles such as CNT and graphene is much higher than that of metal nanoparticles. This implies that the carbon-base nanoparticle have higher potential for enhancing the thermal conductivity of base fluids.^{18,21,22} Among a variety of carbon nanostructures, CNT is a more promising material since they are economically-viable for replacing metallic nanoparticles and graphene.^{23,24} According to the previous studies, CNT showed high thermal conductivity^{4,21,22} as compared with most of the materials, which confirms the potential of CNT for creating thermally conductive nanofluids. Such properties and low cost suggest that CNT is an appropriate candidate for use in

^aDepartment of Mechanical Engineering, University of Malaya, Kuala Lumpur, Malaysia. E-mail: ahm.amiri@gmail.com; ahm.amiri@siswa.um.edu.my; salimnewaz@um.edu.my

^bDepartment of Mechanical and Aeronautical Engineering, Clarkson University, Potsdam, NY 13699, USA

^cDepartment of Chemical Engineering, Faculty of Engineering, Ferdowsi University of Mashhad, Mashhad, Iran. E-mail: mehdi.shanbedi@stu-mail.um.ac.ir

^dDepartment of Chemistry, Faculty of Science, University of Malaya, 50603 Kuala Lumpur, Malaysia

† Electronic supplementary information (ESI) available. See DOI: 10.1039/c5ra02736e

industrial thermal equipment such as car radiators^{25,26} and two-phased closed thermosyphons.^{13,17,27–29} Choi and Eastman¹⁹ showed that CNT-based water nanofluids have higher thermal conductivity compared with pure base fluids. In addition, Choi *et al.*³⁰ revealed that CNT/poly- α -olefin oil improved thermal conductivity approximately 160%. Despite some promising applications of CNT in the field of nanofluids, several issues have limited their thermal applications.

One problem is the tendency of CNT to aggregate and form bundles, which significantly affects the dispersion of CNT in different media. The aggregation phenomenon is due to two important interactions:

- The strong van der Waals interactions among CNT threads.
- The interactions between CNT and the base fluid.

Non-covalent functionalization is an effective approach to improve the dispersibility of CNT.^{4,21,23} However, surfactants might cause some issues such as contamination of the heat transfer media, reducing the effective area of heat transfer, forming foam which consequently causes a disturbance in the setup performance and increasing the thermal resistance between the CNT and the base fluid.²¹ To develop the interactivity, covalent modification was suggested as another solution.^{21,22} In order to enhance dispersibility of CNT in pure water, covalent functionalization using oxidizing acid mixtures has been investigated. Unfortunately, shortening of CNT with oxidizing acid mixtures was a problem and reduced the thermal performance.^{21,31} By synthesizing a nanofluid in this way, stable nanofluids were prepared because the van der Waals forces among nanotubes were removed. To attain a good dispersion in the aqueous media, numerous carboxylic acid groups should be added to the surface of CNT. Frequently, acid-treatment techniques over a long period of time can be used to achieve this goal.³² On the other hand, lots of defects and shortened-length CNT resulted from such techniques, which consequently reduced some thermal properties.^{21,31,32} Although these techniques have been utilized by a majority of thermal scientists as the base-functional group (bridge) for attaching to other functional groups, acidic groups swiftly create a condition that is susceptible for more corrosion. Some other functional groups like different kinds of diamine and ethylene glycol were added to the CNT for enhancing dispersivity in most non-polar and polar solvents.^{23,33} However, majority of the functionalization methods with this approach are comprising of multiple steps and are time-consuming. Some researchers used functional groups with two or more active chains, which can cross-link adjacent CNT. They can behave as a medium to attach adjacent CNT, and finally CNT are interconnected to form aggregates. Also, there are a few functionalized samples that can improve the CNT dispersibility in different base fluids such as water, ethylene glycol (EG), methanol and ethanol.³³ In order to reduce the number of defects and increase the speed and degree of functionalization, the microwave technique along with a non-acidic mixture can be employed.³⁴ Nowadays, the microwave method is recommended as a rapid and environmentally-friendly route to functionalize CNT.^{34,35}

The use of monofunctional tetrahydrofurfuryl-terminated polyethylene glycol (TFPEG) prevents cross-linking of the

adjacent CNT in the final samples, which provides more dispersed CNT in the some base fluids like pure water and EG. Also, in order to decrease the steps of the functionalization, an electrophilic addition reaction under microwave irradiation can be employed as one of the novel methods.³⁶ This procedure can be introduced as a method for industrial scale production of TFPEG-treated CNT and subsequently production of CNT-based water and/or ethylene glycol coolants for heat dissipation applications.

Here, a fast, one-pot and efficient covalent route is employed to synthesize TFPEG-treated multi-walled carbon nanotubes (PMWCNT). An electrophilic addition reaction under microwave irradiation was utilized to synthesize PMWCNT. Also, the mono-functional structure of TFPEG was used to prevent cross-linking among MWCNT, implying higher dispersibility in the polar solutions like water and EG. To prove functionalization, the MWCNT sample was subjected to morphological and chemical characterization. The treated sample was added to the pure water as a base fluid to investigate the thermal properties of PMWCNT-based water nanofluids. Finally, the laminar convective heat transfer and pressure drop of the prepared nanofluids with different weight concentrations were studied at the constant heat flux.

2. Experimental section

2.1. Materials

Pristine MWCNT with diameters less than 30 nm, lengths of 5–15 μm and carbon purity over 95% were purchased from Shenzhen Port Co. Tetrahydrofurfuryl polyethylene glycol ($\text{C}_5\text{H}_9\text{O}(\text{C}_2\text{H}_4\text{O})_{n=2,3}\text{OH}$, MW $\sim 200 \text{ g mol}^{-1}$), AlCl_3 and HCl were obtained from Sigma-Aldrich. *N,N*-Dimethylformamide (DMF) with analytical grade was obtained from Merck Inc.

2.2. Microwave-assisted functionalization

The functionalization procedure of synthesizing PMWCNT is schematically shown in Fig. 1. In a typical experiment, the pristine MWCNT (10 mg) and AlCl_3 as a Lewis acid (0.1 mol) were poured into an agate mortar and were grounded for several minutes. This mentioned mixture and 10 mL TFPEG were then



Fig. 1 Schematic illustration of the functionalization of MWCNT with tetrahydrofurfuryl polyethylene glycol (TFPEG).

poured into a Teflon vessel and sonicated for 30 min at 50 °C until a homogeneous suspension was produced. Afterwards, 0.5 mL concentrated hydrochloric acid was added drop by drop with sonication at 50 °C. The mixture was then heated in an industrial microwave (Milestone MicroSYNTH programmable microwave system) up to 120 °C with output power of 700 W for 30 min. After the reaction was completed, the resulting mixture was cooled to the room temperature, filtered through a thin layer Teflon membrane. In order to remove any unreacted materials, the filter cake was thoroughly washed with DMF and abundant deionized water and then dried under vacuum at 50 °C.

2.3. Preparation of PMWCNT-based water nanofluids

To synthesize PMWCNT-based water nanofluids, PMWCNT were sonicated in a known amount of pure water as a base fluid for nearly 20 min using an ultrasonicator. Unsurprisingly, PMWCNT can easily disperse in the water. The easily-miscible TFPEG functionalities can clarify the higher dispersion of the treated MWCNT (Fig. S₁[†]). The PMWCNT-based water nanofluids were synthesized with weight concentrations of 0.05, 0.1, and 0.2%.

2.4. Thermal apparatus

In the field of heat transfer, the heat transfer coefficient (h) plays the key role in the rate of heat transfer and the performance of thermal equipment. To investigate the thermal properties of samples, a convective heat transfer setup was manufactured, and the schematic is shown in Fig. 2. It had a heat exchanger, pump, flow loop, tank, test section, flow-measuring unit and a differential pressure transducer.

The test section consisted of an adjustable power supply, copper pipe (length of 1.3 m and diameter of 7 mm), three

electrical resistances, two insulation layers, RTD sensors, six K-type thermocouples, and temperature indicators. Six K-type thermocouples were installed in the copper pipe to measure the surface temperature at the different axial distances of 3, 10, 25, 50, 90, and 120 cm from the entrance. Two other PT-100 thermocouples determined the inlet and outlet fluid temperatures of the test section. Also, the precision of the thermocouples were 0.1 °C. The copper pipe and reservoir tank were surrounded uniformly using the insulation layers to enhance validity and decrease the amount of heat loss. A differential pressure transducer was employed to attain the pressure drop of the fluids along the pipe line. Three electrical resistances and power supply were utilized to provide a uniform heat flux around the circular copper pipe. In addition, a pump was used to circulate the fluids, and two valves were installed to adjust the volume flow rate in to the cycle. All tests were carried out in triplicate to improve the accuracy.

2.5. Characterization

Fourier transform infrared spectroscopy, FT-IR, (Nicolet 470 FTIR), Nuclear magnetic resonance spectroscopy, NMR, (FT-NMR LAMBDA 400 MHz, LA 400), Raman spectroscopy (Renishaw confocal spectrometer at 514 nm), thermogravimetric analysis, TGA, (TGA-167 50 Shimadzu), and transmission electron microscopy, TEM, (HT7700, High-Contrast/High-Resolution Digital TEM) were employed to analyse samples. Regarding thermogravimetric analysis (TGA), the mass loss of samples was measured at the heating rate of 10 °C min⁻¹, initial mass of 4 mg and the temperature range of 17–600 °C in air. The preparation of TEM samples comprised of the sonication of GNP in ethanol solution and dropping on a lacey carbon grid and followed by drying under vacuum. The infrared spectra were evaluated in the range of 400–4000 cm⁻¹ and all samples were placed on KBr pellets.

2.6. Data processing

To investigate the influence of the PMWCNT on the thermal properties of pure water, the heat transfer coefficient (h) and the pressure drop (ΔP) may be considered as two critical parameters. The local heat transfer coefficient ($h(x)$) at an axial distance 'x' from inlet is given as:

$$h(x) = \frac{q}{T_w(x) - T_b(x)} \quad (1)$$

where q , $T_w(x)$ and $T_b(x)$ are heat flux and wall and fluid bulk temperature at a distance "x" from the inlet, respectively. The heat flux (q) was obtained using:

$$q = \frac{Q}{\pi D x} \quad (2)$$

The parameter of Q is the power provided by the power supply. The bulk temperature of the fluid was calculated at the axial distance of 'x' as:³⁷

$$T_b(x) = T_{in} + \frac{q\pi D x}{m^{\circ} C_p} \quad (3)$$

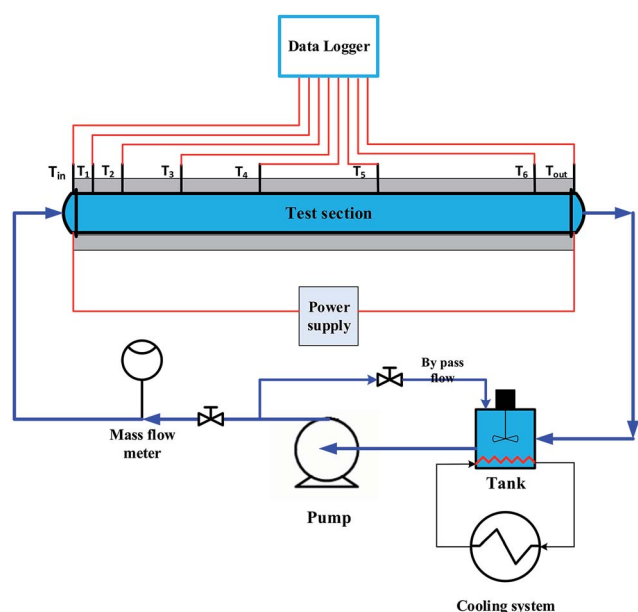


Fig. 2 Schematic of the convective heat transfer loop.

Table 1 The thermal conductivity of PMWCNT-based water nanofluids at different temperature and weight concentrations

Thermal conductivity ($\text{W m}^{-1} \text{K}^{-1}$)				
T ($^{\circ}\text{C}$)	Water	0.05% wt PMWCNT	0.1% wt PMWCNT	0.2% wt PMWCNT
30	0.601	0.623	0.651	0.686
40	0.624	0.543	0.672	0.704
50	0.642	0.654	0.689	0.736
60	0.653	0.669	0.696	0.751

Previously, some correlations such as Xue^{38–40} and Nan and Lin⁴¹ were suggested to calculate the thermal conductivity of the PMWCNT-based water nanofluids and some other nanofluids. However, they did not consider the effect of different functional groups the weight ratio of functionality to carbon. Thus, in this study, thermal conductivity of samples was measured experimentally to avoid any uncertainty. To increase the validity of results, the thermal conductivity of PMWCNT-based water nanofluids, recorded with a KD2 Pro thermal analyzer (Decagon Devices, USA), was recorded at different temperatures and weight concentrations as shown in Table 1. It can be seen that as the temperature and weight concentration of PMWCNT increased, thermal conductivity increased.

In addition, the viscosity of PMWCNT-based water nanofluid (μ_{nf}) is calculated by the correlation of Brinkman:⁴²

$$\mu_{\text{nf}} = \frac{1}{(1 - \phi)^{2.5}} \mu_{\text{b}} \quad (4)$$

In order to obtain the density of nanofluids, the mixture model⁴³ is used. That is,

$$\rho_{\text{nf}} = \phi \rho_{\text{p}} + (1 - \phi) \rho_{\text{b}} \quad (5)$$

The Reynolds number was calculated using:

$$\text{Re} = \frac{\rho U D}{\mu} \quad (6)$$

Also, the pressure drop of pure water at different Reynolds numbers was calculated using:

$$\Delta P = \frac{32 \mu_{\text{nf}} U L}{D^2} \quad (7)$$

The uncertainties of the experiments were obtained by the Holman method⁴⁴ as follows:

$$\text{Max}E_{\text{h}} = \pm[(E_{\text{Q}})^2 + (-E_{\text{A}})^2 + (-E_{(T_{\text{w}} - T_{\text{b}})})^2]^{1/2} \quad (8)$$

$$\text{Max}E_{\text{Q}} = \pm[(E_{\text{V}})^2 + (E_{\text{I}})^2]^{1/2} \quad (9)$$

$$\text{Max}E_{\text{A}} = \pm[(-E_{\text{D}})^2 + (-E_{\text{X}})^2]^{1/2} \quad (10)$$

$$\text{Max}E_{\Delta P} = \pm[(E_{\mu_{\text{nf}}})^2 + (E_{\text{U}})^2 + (E_{\text{L}})^2 + 2(-E_{\text{D}})^2]^{1/2} \quad (11)$$

Finally, the maximum uncertainty of the heat transfer coefficient and pressure drop are less than 5.5 and 5 respectively.

3. Results and discussion

3.1. Functionalization study

In the field functionalization, the covalent functionalization of MWCNT with TFPEG was reported by Kalinina *et al.*³³ Here, tetrahydrofurfuryl polyethylene glycol (TFPEG) was used as a monofunctional oligomer in order to prevent cross-linking among the CNT.³³ It is noteworthy that TFPEG can be also utilized as a function in order to disperse MWCNT in water and EG, which has been used as the base fluids in a majority of thermal equipment such as car radiators. In addition, TFPEG has no destructive effects such as corrosion or foaming in the thermal equipment. In addition, a microwave-assisted method is introduced for functionalization of MWCNT *via* TFPEG in order to provide an effective, economical and rapid method. Thus, in order to confirm this functionalization procedure and investigate the degree of functionalization, qualitative (FT-IR) and quantitative (thermogravimetric analysis (TGA) and Raman spectroscopy) characterizations have been employed.

3.1.1. Fourier transform infrared spectroscopy. As noted before, TFPEG can enhance the dispersibility of CNT in aqueous media.³³ Here an electrophilic addition reaction was utilized to speed the reaction between MWCNT and TFPEG under microwave irradiation. Fig. 3 illustrates the FT-IR spectra of PMWCNT and pristine MWCNT in transmittance (%) *vs.* wavenumber (cm^{-1}). In contrast to the pristine sample, the PMWCNT demonstrates the cues of TFPEG molecules on the MWCNT structures. A detailed list of the main infrared peaks along with their assigned bonds is given in Table 2. According to Fig. 3, PMWCNT shows significant peaks of C–O, CH_2 , and C–H bonds. The mentioned bonds correspond to attaching TFPEG on the MWCNT surface. It is noteworthy that the PMWCNT sample represents a specific peak in the range of 3000 to 3500 cm^{-1} , which confirms the presence of –OH groups on the surface of MWCNT.^{33,35}

To evaluate the degree of functionalization, the quantitative tests (Raman spectroscopy and TGA) have been applied to provide additional evidences.

Raman spectroscopy was also employed to provide basic information for studying the covalent functionalization of MWCNT. Raman characterization was determined by an

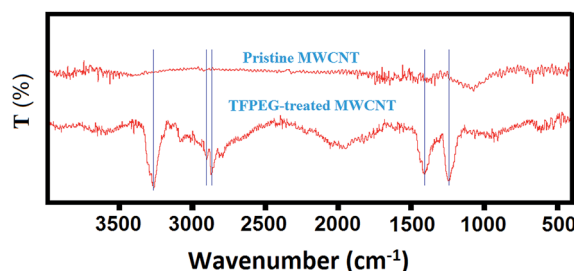


Fig. 3 FTIR spectra of pristine and TFPEG-treated MWCNT.

Table 2 Fourier transform infrared interpretation of the TFPEG-treated MWCNT

Peak (cm ⁻¹)	Interpretation	T%
1213	C–O stretching vibration	25.47 (S)
2800–2850	C–H stretching vibration and asymmetric stretching of CH ₃	32.48 & 49.68 (M)
1398	CH ₂ bending vibration	33.12 (M)
3000–3500	–OH stretching vibration	17.19 (S)

eminent sensitivity to the disordered band on the structure depending upon the optical skin depth.^{45,46} Therefore, the Raman spectra of the pristine MWCNT and PMWCNT are shown in Fig. S₂.† It can be seen that the intensity ratios (I_D/I_G)

of PMWCNT is higher than that of the pristine MWCNT, which can be an evidence for functionalization of MWCNT with TFPEG and/or inducing defects in CNT by sonication.^{47,48}

3.1.2. NMR spectroscopy. The ¹H NMR spectrum of TFPEG-treated MWCNT suspension in CDCl₃ in a high-field region (Fig. 4) contains signals of the hydrogen atoms of the TFPEG substituent.

The sharp signal at δ_H 3.645 is characteristic of TFPEG-treated MWCNT, which is attributed to the surface alcohol groups (OH) formed during the chemical modifications.

The ¹H NMR spectra results of analyses of the addition product of TFPEG to the MWCNT surface are given in Table 3.

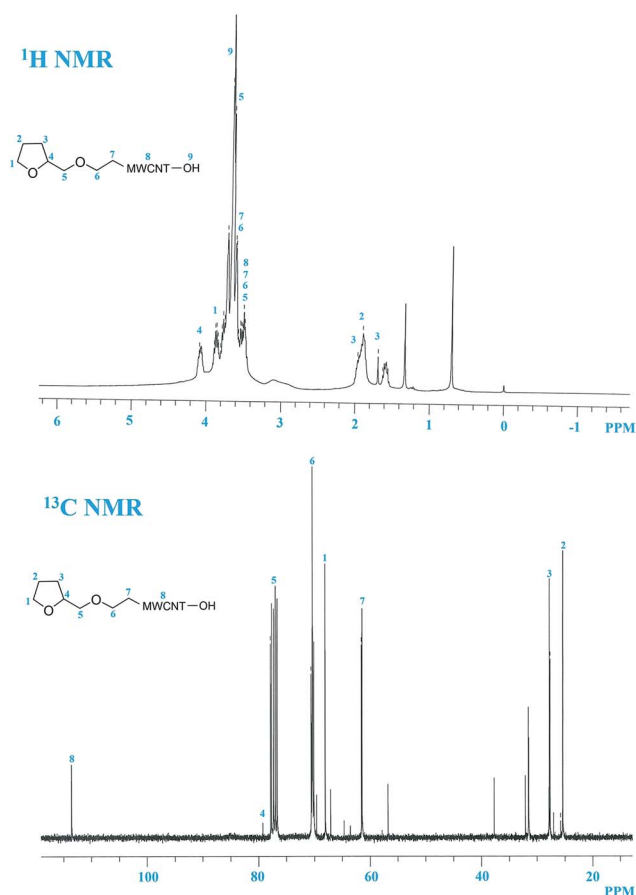
The ¹³C NMR spectrum and results of TFPEG-treated MWCNT are given in Fig. 4 and Table 3, respectively. The resonance region of TFPEG-treated MWCNT contains signals from the aromatic furan and methylene groups. Overall, NMR results suggest some results as follow:

-Functionalization of MWCNT with TFPEG was successful.

-The presence of furan signals could be an indicative of the lack of ring-opening reaction (Friedel–Crafts acylation).

-A broad signal at δ_H 3.55 is attributed to the methylene group, which can be an evidence for the presence of linkage between MWCNT surface and TFPEG. Also, a peak at 3.55 can be attributed to the protons on MWCNT surface.⁴⁹

3.1.3. Thermogravimetric analysis. TGA provides the valuable information about the quantitative amount of functional groups on MWCNT surface. Fig. 5 illustrates evidence of the functionalization of MWCNT with TFPEG. As can be seen in Fig. 5, the TGA curve of the pristine sample depicts no significant mass loss up to 500 °C which is attributed to the thermal degradation of the main graphitic structures. On the other hand, PMWCNT illustrates two noticeable mass losses in the temperature range of 0–600 °C. Consistent with the curve of PMWCNT, the mild mass loss (the first weight loss) in the

Fig. 4 ¹H NMR and ¹³C NMR spectra of TFPEG-treated MWCNT.Table 3 Results of ¹H NMR and ¹³C NMR spectroscopy of TFPEG-treated MWCNT

Position	¹ H NMR (chemical shift)	DEPT	¹³ C NMR (chemical shift)	DEPT
1	3.7 & 3.8	CH ₂ (protons of tetrahydrofuran)	67.9	CH ₂ (tetrahydrofuran)
2	1.8 & 1.9	CH ₂ (protons of tetrahydrofuran)	25.88	CH ₂ (tetrahydrofuran)
3	1.69 & 1.96	CH ₂ (protons of tetrahydrofuran)	27.69	CH ₂ (tetrahydrofuran)
4	4.07	CH (protons of tetrahydrofuran)	77.8	CH (tetrahydrofuran)
5	3.48 & 3.61	CH ₂ (protons of methylene)	76.6	CH ₂ (aliphatic)
6	3.47 & 3.59	CH ₂ (protons of methylene)	70.56	CH ₂ (aliphatic)
7	3.46 & 3.57	CH ₂ (protons of methylene)	61.35	CH ₂ (aliphatic)
8	3.55	Protons of benzene rings of MWCNT	113.59	C=C of benzene rings of MWCNT
9	3.64	OH (alcohol)	—	—

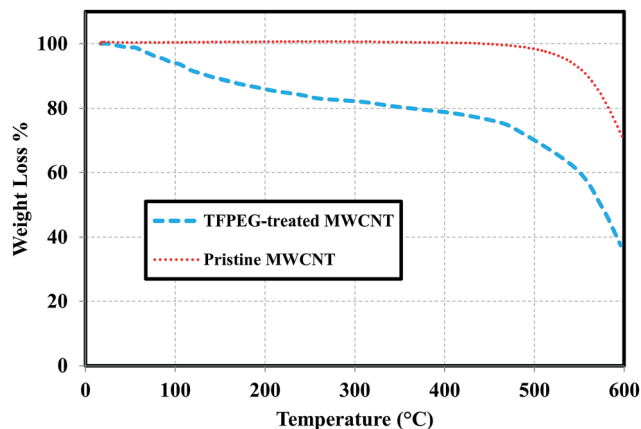


Fig. 5 Thermogravimetric analysis of the pristine and TFPEg-treated MWCNT.

temperature range of 100–150 °C is related to the functionality of TFPEg as an unstable organic moiety on MWCNT. TGA results confirm that MWCNT was successfully functionalized *via* a monofunctional oligomer (TFPEg), which is in agreement with the increased I_D/I_G observed in the Raman spectra of the pristine and treated samples. Moreover, the second mass loss around 500 °C is associated with the degradation temperature of the main graphitic structures in air.⁵⁰

3.1.4. TEM microscopy. TEM images of the PMWCNT and pristine sample are shown in Fig. 6A. In the pristine MWCNT image (Fig. 6A), one can see multi-walled CNT with relatively smooth and intact walls and low wall-defected CNT. On the other hand, cut and open ends of MWCNT are obvious after treatment, which could be the result from the severe functionalization condition under microwave irradiation. Moreover, Fig. 6B and C depict the high surface roughness for the PMWCNT. This surface roughness can be the result from the partial damage of graphitic carbon that occurred due to the

severe condition of functionalization. In fact, the sp^2 carbon in the graphitic network of MWCNT disrupted during the functionalization procedure can be the main reason for the surface's deterioration, which is in agreement with the higher I_D/I_G in the Raman results. In addition, the easily miscible TFPEg functionalities on MWCNT in water can elucidate the excellent dispersion of the PMWCNT (ESI, Fig. S1†).

3.2. Thermal analysis

3.2.1. Accuracy. To evaluate the accuracy and reliability of the experimental system before conducting systematic experiments with PMWCNT-based water nanofluids, pure water was tested as the base fluid and compared with the reported equation. The experimental heat transfer coefficients of the pure water at different values of x/D were employed as an excellent parameter for comparison. The results are presented in Fig. 7, along with predictions of the common Shah equation for laminar flows over the constant heat flux boundary condition.⁵¹ As can be seen in Fig. 7, the predicted heat transfer coefficients by the Shah equation is in good agreement with the experimental data over the Reynolds number range used in this work, which verified the accuracy of the apparatus.

Eqn (12) demonstrates Shah's correlation.

$$Nu = \begin{cases} 1.953 \left(Re \times Pr \frac{D}{x} \right)^{1/3} & \left(Re \times Pr \frac{D}{x} \right) \geq 33.3 \\ 4.364 + 0.0722 \left(Re \times Pr \frac{D}{x} \right) & \left(Re \times Pr \frac{D}{x} \right) < 33.3 \end{cases} \quad (12)$$

3.2.2. Convective heat transfer coefficient of PMWCNT-based water nanofluids. With the confirmed accuracy of the experimental approach, systematic tests were carried out at various Reynolds numbers (in laminar flow range) and different

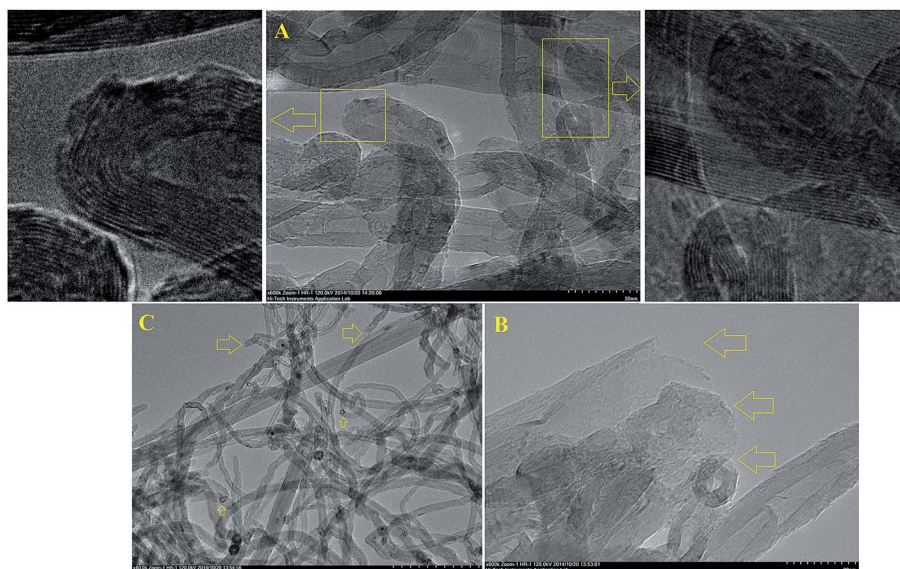


Fig. 6 TEM microscopy of the (A) pristine and (B and C) TFPEg-treated MWCNT.

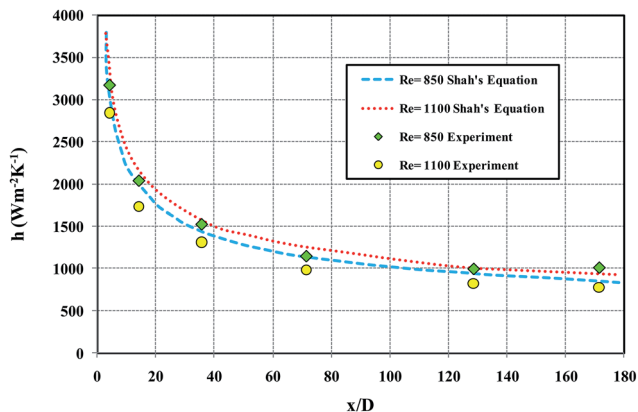


Fig. 7 Initial test of the convective heat transfer loop using distilled water.

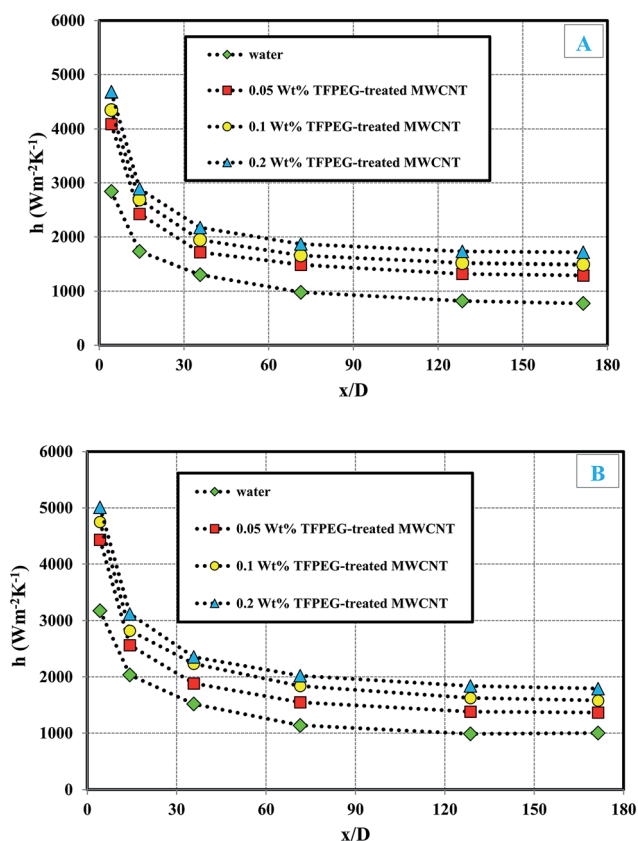


Fig. 8 Heat transfer coefficients of PMWCNT-based water nanofluids at different concentrations as well as pure water at (A) $Re = 800 \pm 50$ and (B) $Re = 1100 \pm 50$.

PMWCNT concentrations. Fig. 8a and b illustrate the influence of PMWCNT concentration on the local heat transfer coefficient at different axial distances from the entrance of the test section at $Re = 800 \pm 50$ and $Re = 1100 \pm 50$, respectively. Also, the results for distilled water are presented in Fig. 8 for comparison purposes. As can be seen, the curve of pure water is under the three curves of PMWCNT-based water nanofluids at different axial distances, three concentrations and both Reynolds numbers. This figure confirms that the addition of MWCNT

into the water enhances the convective heat transfer coefficient. As a result, as the weight concentration of MWCNT increases, the convective heat transfer coefficient at different axial distances from the inlet of the test section increases. For example, at the Reynolds number of 1100 ± 50 and x/D of 71.428, by increasing the weight concentration from 0.05 to 0.2%, the convective heat transfer coefficient increases from 1549 to $2021 \text{ W m}^{-2} \text{ K}^{-1}$. Indeed, this change in MWCNT weight concentration from 0.05% to 0.2% enhances the convective heat transfer coefficient more than 30%. The presence of MWCNT enhances the convective heat transfer coefficient considerably and the ratio of growth is approximately similar as the concentration increases. The increasing of Nusselt number with the increasing of Reynolds number can be also attributed to the increasing of fluid thermal conductivity.

In addition, the heat transfer coefficient shows a downward trend with axial distance at a constant concentration of PMWCNT, which is an expected trend.^{51,52} The reported results confirm that the development of the convective heat transfer coefficient with change in axial distance is significant and is attributed to the improvement of thermal conductivity of base fluid in the presence of nanostructures.^{21,22,52} Xuan and Li⁵³ showed that the heat transfer coefficient increases by 60% in the presence of Cu-based water nanofluids nanofluid with copper concentration of 2%. Again, as the thermal conductivity of nanoparticles in base fluids increases, the thermal boundary-layer thickness decreases, which results in an increasing convective heat transfer coefficient.^{22,24}

In order to provide a better comparison and investigate the influence of a PMWCNT addition on the convective heat transfer coefficient, the enhancement of the convective heat transfer coefficient with reference to the distilled water is studied at different weight concentrations and $Re = 800 \pm 50$ and $Re = 1100 \pm 50$, which are shown in Fig. S₃ (ESI[†]). Overall, the results show that all synthesized samples have an excellent potential to transfer heat in thermal equipment and confirm the positive effect of covalent functionalization on the thermal performance of various setups.

Fig. 9 illustrates the influence of the Reynolds number on the convective heat transfer coefficient, which obviously is shown as an upward trend with increasing Reynolds number at constant weight concentration of 0.1%. First, it can be seen that the convective heat transfer increases with increasing Reynolds number. For example, at x/D of 71.428, an increase in Reynolds number from 800 to 2000 results in improvement of the convective heat transfer coefficient from 1655.8 to 2673.9, which shows 61.4% growth. Also, there is a great difference between the convective heat transfer coefficient at $Re = 1100$ and that at $Re > 1500$. At all x/D , the enhancement for $Re = 1500$ is higher than that for $Re = 1100$ and 800. Ding *et al.*⁵² reported that the influence of Reynolds number on convective heat transfer coefficient is small at $Re < 1100$; however, a significant growth can be obtained at Reynolds numbers higher than 1100. They concluded that the shear rate at the wall is around 500 s^{-1} at $Re = 1100$, which they attributed to the change from the strong shear thinning region to the region with constant viscosity. Similarly, Fig. S₄[†] illustrates the measured Nusselt number of the

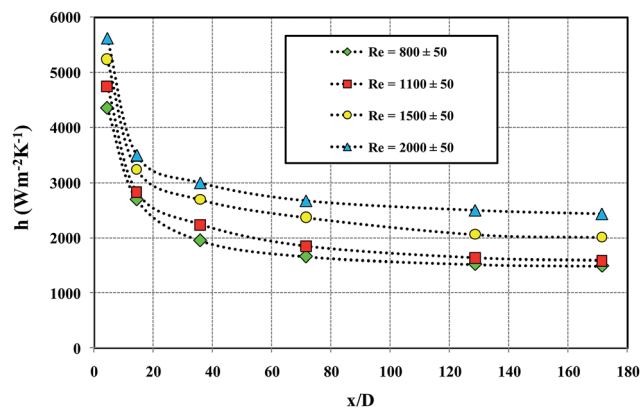


Fig. 9 Heat transfer coefficients of PMWCNT-based water nanofluids at constant weight concentration of 0.1% at different Re numbers.

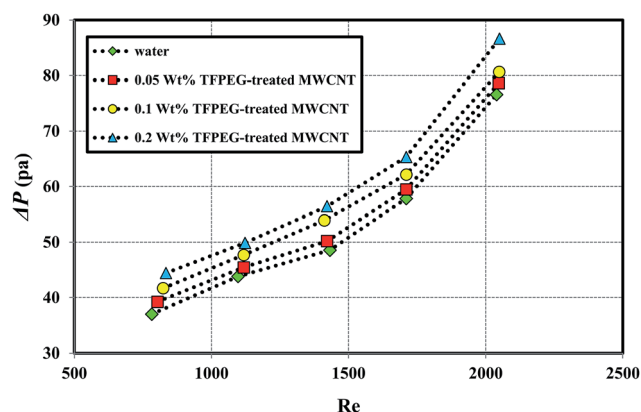


Fig. 10 Effect of Reynolds number and concentration of PMWCNT-based water nanofluids on the pressure drop.

PMWCNT-based water nanofluids at weight concentration of 0.1% for different Reynolds numbers. It is observed that the Nusselt number decreases quickly with the increase in x/D . Also, as the Reynolds number increases, the Nusselt number increases.

3.2.3. Pressure drop. Fig. 10 shows the pressure drop of pure water and PMWCNT-based water nanofluids *versus* Reynolds number in various weight concentrations. It can be seen that the pressure drop of PMWCNT-based water nanofluids increases continuously with increasing PMWCNT concentration and Reynolds number, in which the dependence of the pressure drop on Reynolds number is almost linear. According to the results, the highest increase in pressure drop of PMWCNT-based water nanofluids is obtained at the weight concentration of 0.2% and $Re = 2000 \pm 50$. As compared to the pure water, the maximum increase in the pressure drop in the presence of MWCNT is about 13%. That is, the higher weight concentration of PMWCNT in the base fluids means the higher viscosity, implying more pressure drop.⁴

4. Conclusions

In this study, a simple and cost-effective method that included the use of microwave irradiation was used to functionalize

MWCNT with TFPEG. In addition, an electrophilic reaction under microwave irradiation was utilized to speed up the functionalization procedure, which resulted in the high-performance reaction as well as excellent solubility in water.

According to the characterization and morphology results, functionalization of MWCNT with TFPEG was successful. As the functionalization was carried out, the stability of PMWCNT in water increased significantly. PMWCNT-based water nanofluids with different weight concentrations were synthesized and their convective heat transfer coefficient and pressure drop under laminar flow condition were investigated.

Based on the presented results, the following conclusions are drawn:

- Covalent functionalization *via* TFPEG under microwave irradiation along with an electrophilic reaction may be used as an economical method to synthesize PMWCNT-based water nanofluids with high dispersibility and stability in aqueous media.

- As the MWCNT concentration increases, the convective heat transfer coefficient is enhanced at various Reynolds numbers in the laminar flow regime.

- At constant weight concentration, as the Reynolds number increases, the convective heat transfer coefficient increases.

- The enhancement of the convective heat transfer coefficient with reference to the distilled water demonstrates that PMWCNT-based water nanofluids with various weight concentrations would be an appropriate operating fluid at different Reynolds numbers.

- The improvement of heat transfer at various weight concentrations of PMWCNT was attributed to the decrease in the thermal boundary layer thickness.

- Results show that the pressure drop increases with weight concentration of MWCNT and flow Reynolds number, although the influence of weight concentration is small.

The effective and promising microwave-assisted method for preparing PMWCNT-based water nanofluids results in excellent stability, non-acidic environments, and a high convective heat transfer coefficient. These findings suggest that the PMWCNT-based water nanofluids can be used as effective coolants in heat transfer equipment.

Nomenclature

C_p	Specific heat, $J\ kg^{-1}\ K^{-1}$
D	Tube diameter, m
h	Heat transfer coefficient, $W\ m^{-2}\ K^{-1}$
k	Thermal conductivity, $W\ m^{-1}\ K^{-1}$
L	Tube length, m
m°	Mass flow rate, $kg\ s^{-1}$
Nu	Nusselt number
Pr	Prandtl number
q	Heat flux, $W\ m^{-2}$
Q	Heat transfer rate, W
Re	Reynolds number
T	Temperature, $^{\circ}C$

Paper

U	Velocity, m s^{-1}
x	Axial distance, m

Greek symbols

φ	Volume fraction
ρ	Density, kg m^{-3}
μ	Fluid viscosity, Pa s
ε	Performance index
ΔP	Pressure drop

Subscripts

b	Bulk fluid
in	Inlet
nf	Nanofluid
p	Particles
w	Wall

Acknowledgements

The authors gratefully acknowledge Bright Sparks Unit of the University of Malaya, UMRG Grant RP012B-13AET and High Impact Research Grant UM.C/625/1/HIR/MOHE/ENG/45, Faculty of Engineering, University of Malaya, Malaysia for support to conduct this research work.

References

- 1 Y. Xuan, H. Duan and Q. Li, *RSC Adv.*, 2014, **4**, 16206–16213.
- 2 M. Rashidi, S. Abelman and N. F. Mehr, *Int. J. Heat Mass Transfer*, 2013, **62**, 515–525.
- 3 H. Yarmand, G. Ahmadi, S. Gharekhani, S. N. Kazi, M. R. Safaei, M. S. Alehashem and A. B. Mahat, *Entropy*, 2014, **16**, 6116–6132.
- 4 A. Amiri, R. Sadri, M. Shanbedi, G. Ahmadi, B. Chew, S. Kazi and M. Dahari, *Energy Convers. Manage.*, 2015, **92**, 322–330.
- 5 M. Rashidi, M. Rastegari, M. Asadi and O. A. Bég, *Chem. Eng. Commun.*, 2012, **199**, 231–256.
- 6 T. S. Sreeremya, A. Krishnan, L. N. Satapathy and S. Ghosh, *RSC Adv.*, 2014, **4**, 28020–28028.
- 7 W. Cui, Z. Shen, J. Yang, S. Wu and M. Bai, *RSC Adv.*, 2014, **4**, 55580–55589.
- 8 K. Balamurugan, P. Baskar, R. Mahesh Kumar, S. Das and V. Subramanian, *J. Phys. Chem. C*, 2012, **116**, 4365–4373.
- 9 O. Mahian, A. Kianifar, C. Kleinstreuer, M. D. A. Al-Nimr, I. Pop, A. Z. Sahin and S. Wongwises, *Int. J. Heat Mass Transfer*, 2013, **65**, 514–532.
- 10 S. Z. Heris, M. Fallahi, M. Shanbedi and A. Amiri, *Heat Mass Transfer*, 2015, DOI: 10.1007/s00231-015-1548-9.
- 11 O. Mahian, S. Mahmud and S. Wongwises, *J. Thermophys. Heat Transfer*, 2012, **27**, 161–169.
- 12 A. Amiri, M. Shanbedi, H. Amiri, S. Z. Heris, S. Kazi, B. Chew and H. Eshghi, *Appl. Therm. Eng.*, 2014, **71**, 450–459.
- 13 M. Shanbedi, S. Z. Heris, A. Amiri and M. Baniadam, *J. Dispersion Sci. Technol.*, 2014, **35**, 1086–1096.
- 14 S. U. S. Choi and J. A. Eastman, *Enhancing thermal conductivity of fluids with nanoparticles*, 1995.
- 15 S. U. S. Choi, in *International Mechanical Engineering Congress and Exposition*, 1995.
- 16 S. S. J. Aravind and S. Ramaprabhu, *RSC Adv.*, 2013, **3**, 4199–4206.
- 17 M. Shanbedi, S. Zeinali Heris, M. Baniadam and A. Amiri, *Exp. Heat Transfer*, 2013, **26**, 26–40.
- 18 M. Azizi, M. Hosseini, S. Zafarnak, M. Shanbedi and A. Amiri, *Ind. Eng. Chem. Res.*, 2013, **52**, 10015–10021.
- 19 S. U. S. Choi and J. A. Eastman, *U.S. Pat.* 6,221,275., April 24, 2001.
- 20 S. Z. H. S. H. Noie, M. Kahani and S. M. Nowee, *Int. J. Heat Fluid Flow*, 2009, **30**, 700–705.
- 21 A. Amiri, M. Shanbedi, H. Eshghi, S. Z. Heris and M. Baniadam, *J. Phys. Chem. C*, 2012, **116**, 3369–3375.
- 22 S. S. J. Aravind, P. Baskar, T. T. Baby, R. K. Sabareesh, S. Das and S. Ramaprabhu, *J. Phys. Chem. C*, 2011, **115**, 16737–16744.
- 23 M. M. A. Amiri, M. Baniadam and S. Zeinali Heris, *Appl. Surf. Sci.*, 2011, **257**, 10261–11026.
- 24 T. T. Baby and S. Ramaprabhu, *J. Mater. Chem.*, 2011, **21**, 9702–9709.
- 25 A. M. Hussein, R. A. Bakar, K. Kadrigama and K. V. Sharma, *Int. Commun. Heat Mass Transfer*, 2014, **53**, 195–202.
- 26 A. Hussein, R. A. Bakar, K. Kadrigama and K. V. Sharma, *Heat Mass Transfer*, 2014, **50**, 1553–1561.
- 27 M. Shanbedi, S. Z. Heris, M. Baniadam, A. Amiri and M. Maghrebi, *Ind. Eng. Chem. Res.*, 2012, **51**, 1423–1428.
- 28 M. Shanbedi, A. Amiri, S. Rashidi, S. Z. Heris and M. Baniadam, *Heat Transfer Eng.*, 2015, **36**, 315–324.
- 29 S. Z. Heris, M. Shokrgozar, S. Poorpharhang, M. Shanbedi and S. H. Noie, *J. Dispersion Sci. Technol.*, 2013, **35**, 677–684.
- 30 S. U. S. Choi, Z. G. Zhang, W. Yu, F. E. Lockwood and E. A. Grulke, *Appl. Phys. Lett.*, 2001, **79**, 2252–2254.
- 31 V. Datsyuk, M. Kalyva, K. Papagelis, J. Parthenios, D. Tasis, A. Siokou, I. Kallitsis and C. Galiotis, *Carbon*, 2008, **46**, 833–840.
- 32 L. Qingwen, Y. Hao, Y. Yinchun, Z. Jin and L. Zhongfan, *J. Phys. Chem. B*, 2002, **106**, 11085–11088.
- 33 I. Kalinina, K. Worsley, C. Lugo, S. Mandal, E. Bekyarova and R. C. Haddon, *Chem. Mater.*, 2011, **23**, 1246–1253.
- 34 E. Vázquez and M. Prato, *ACS Nano*, 2009, **3**, 3819–3824.
- 35 H. Z. Zardini, A. Amiri, M. Shanbedi, M. Maghrebi and M. Baniadam, *Colloids Surf., B*, 2012, **92**, 196–202.
- 36 R. Tian, X. Wang, M. Li, H. Hu, R. Chen, F. Liu, H. Zheng and L. Wan, *Appl. Surf. Sci.*, 2008, **255**, 3294–3299.
- 37 K. Tumuluri, J. L. Alvarado, H. Taherian and C. Marsh, *Int. J. Heat Mass Transfer*, 2011, **54**, 5554–5567.
- 38 Q. Xue, *Phys. B*, 2005, **368**, 302–307.
- 39 Q. Xue, *Nanotechnology*, 2006, **17**, 1655.
- 40 Q.-Z. Xue, *Phys. Lett. A*, 2003, **307**, 313–317.

- 41 C.-W. Nan, Z. Shi and Y. Lin, *Chem. Phys. Lett.*, 2003, **375**, 666–669.
- 42 H. C. Brinkman, *J. Chem. Phys.*, 1952, **20**, 571.
- 43 B. C. Pak and Y. I. Cho, *Exp. Heat Transfer*, 1998, **11**, 151–170.
- 44 J. P. Holman, *Heat Transfer*, McGraw-Hill, New York, 5th edn, 1981.
- 45 A. Amiri, M. Memarpoor-Yazdi, M. Shanbedi and H. Eshghi, *J. Biomed. Mater. Res., Part A*, 2013, **101A**, 2219–2228.
- 46 A. Amiri, H. Z. Zardini, M. Shanbedi, M. Maghrebi, M. Baniadam and B. Tolueinia, *Mater. Lett.*, 2012, **72**, 153–156.
- 47 S. D. M. Brown, A. Jorio, M. S. Dresselhaus and G. Dresselhaus, *Phys. Rev. B: Condens. Matter Mater. Phys.*, 2001, **64**, 073403.
- 48 Z. D. Liu, Y. Feng and W. L. Li, *RSC Adv.*, 2015, **5**, 29017–29021.
- 49 A. S. Ivanov, S. V. Savilov, M. N. Kirikova and V. V. Lunin, *Russ. Chem. Bull.*, 2012, **61**, 1882–1891.
- 50 H. Z. Zardini, M. Davarpanah, M. Shanbedi, A. Amiri, M. Maghrebi and L. Ebrahimi, *J. Biomed. Mater. Res., Part A*, 2014, **102**, 1774–1781.
- 51 R. K. Shah, *3rd National Heat Mass Transfer Conference*, Indian Institute of Technology, 1975, HMT-11–75.
- 52 Y. Ding, H. Alias, D. Wen and R. A. Williams, *Int. J. Heat Mass Transfer*, 2006, **49**, 240–250.
- 53 Y. Xuan and Q. Li, *Int. J. Heat Fluid Flow*, 2000, **21**, 58–64.